PriMera Scientific Engineering
Volume 5 Issue 3 September 2024
DOI: 10.56831/PSEN-05-150
ISSN: 2834-2550

PriMera Scientific Publications

Design Study of high-power PV grid-connected Inverter System based on the Particle Swarm Algorithm

Type: Research Article
Received: August 02, 2024
Published: August 08, 2024

Citation:
Noppadol Amdee., et al. "Design Study of high-power PV grid-connected Inverter System based on the Particle Swarm Algorithm". PriMera Scientific Engineering 5.3 (2024): 16-38.

Qinghe Xu, Noppadol Amdee* and Adisak Sangsongfa

Doctor of Industrial Technology Management, Faculty of Industrial Technology, Muban Chom Bueng Rajabhat University, Thailand

***Corresponding Author:** Noppadol Amdee, Doctor of Industrial Technology Management, Faculty of Industrial Technology, Muban Chom Bueng Rajabhat University, Thailand.

Abstract

Photovoltaic (PV) power generation is an essential form of renewable energy. A grid-connected PV inverter is the core equipment of a grid-connected PV power generation system. Based on the working principle of a high-power PV grid-connected inverter, the design of a 500 kW PV grid-connected inverter system is considered as an example. The equipment selection and parameter design methods of critical components, such as DC support capacitors, DC to AC modules, inductors, and capacitors, are introduced, and the overall system control strategy scheme and maximum power point tracking strategy are proposed. The results of MATLAB system simulation and field measurement experiments show that the control system can ensure that the output three-phase voltage and current are always in the same phase and frequency and that the output power is stable, fully meeting the grid connection requirements. In addition, the system has high conversion efficiency, good harmonic suppression, and a good MPPT tracking effect based on the particle swarm algorithm, which has high application and promotion value.

Keywords: Grid-connected inverter; Harmonic; System Design; MPPT; Conversion efficiency; Particle swarm algorithm

Introduction

In recent years, with the rapid development of the overall solar industry technology, Photovoltaic (abbreviated as PV) power generation has become an essential supplement to energy supply. The rapid introduction of the de-subsidization policy has led to a rapid decline in the price of the entire industry chain; the installed capacity of PV power plants is increasing, and PV power generation is heading toward the stage of grid parity. In the parity stage, the performance requirements, reliability requirements, and stability requirements of inverters for PV power generation in the grid parity stage are stricter. There are four main classifications of PV grid-connected inverters: single-phase inverters [1] and three-phase inverters [2], according to the number of phases of inverter output. Isolated inverters and non-isolated inverters [3] according to the internal transformer or not; Single-stage inverters, dual-stage inverters, and multi-stage inverters according to the number of system power

conversion stages. PV inverters can also be classified into centralized inverters [4], string inverters, and micro-inverters according to the applicable power level of the PV inverter. These different types of inverters are suitable for various applications, considering factors such as operation and maintenance costs, system power generation, and stability of grid-connected power generation.

Under the influence of these comprehensive factors, the construction scale of large-scale photovoltaic power plants is rapidly expanding, and high-power centralized grid-connected inverters are widely used. In this study, based on analyzing the working principle of a high-power three-phase PV grid-connected inverter, a 500KW PV grid-connected inverter with an isolation transformer is designed and simulated [5], and field experiments are carried out in terms of both hardware design and software control strategy. The experimental results show that the inverter is reasonable in design, reliable in operation, meets all the design indexes, and has high application and promotion value.

Basic Working Principle

A grid-connected PV system is a PV power generation system that connects to and transmits electricity to the grid. Through the PV panel module, the received solar radiation energy was transformed into high-voltage direct current (DC) power after high-frequency DC conversion, and each branch DC was connected to the DC input side of the grid-connected inverter after the convergence box and DC distribution. The grid-connected inverter is the core of the PV grid-connected power generation system. It converts power from the PV array into sinusoidal AC currents matching the grid voltage frequency and phase by inverting IGBT power-switching devices.

The center circuit topology of the 500 kW three-phase PV grid-connected inverter is shown in Fig. 1. The DC part is the PV panel, EMC is the filter, C1 is the support capacitor, L1 is the inductor, and C2, C3, and C4 are the delta capacitors. The three-phase full-bridge inverter circuit adopts a single-stage transformer LC filter structure. The AC side outputs a three-phase modulated voltage, and the current is filtered by the LC filter and connected to the grid.

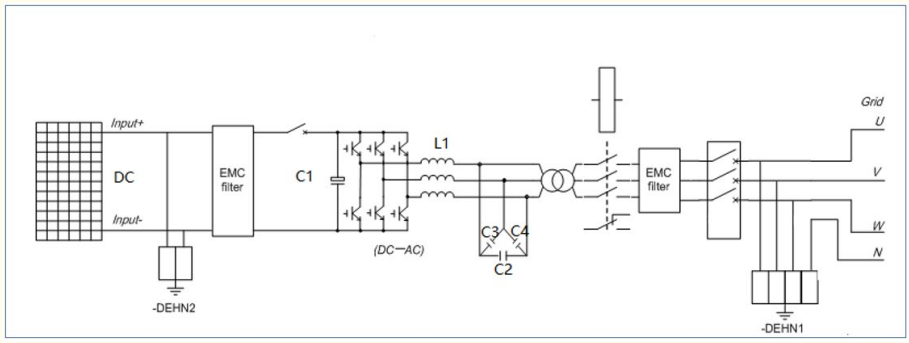

Figure 1: Topology of the primary circuit of the grid-connected inverter.

Design of Key Component Parameters

DC Support Capacitor Design

The primary function of the DC support capacitor (C1 in Figure 1) is to support the DC voltage, maintain a stable DC voltage, and filter out the low harmonic current in the DC voltage. Considering the ripple up and down 15V, take the DC side voltage as 400V. The maximum ripple voltage U_{max} =415V, the minimum ripple voltage U_{min} = 385V, then the 500 kW DC side support capacitor is selected based on formula (1) as follows:

$$C_{\min} = \frac{P}{(U_{\max}^2 - U_{\min}^2) \times f \times \eta} \qquad (1)$$

where P is the frontal power of the inverter, P =500KW, f is the switching frequency, f =3000 Hz, η is the whole efficiency of the inverter, take η =0.985, so C_{min} =7050uF.

From the ripple current calculation formula.

$$I_{res} = \frac{P}{(U_{\max} + U_{\min}) \times 0.5} \quad (2)$$

Got. I_{res} =1250A.

From the three aspects of DC measurement voltage, ripple current, and minimum support capacitor value, the DC support capacitor of this system is EACO 30 SHE-1000-350 in parallel. The total capacitance is C = 350 × 30 = 10500uF, 350 is the capacitance of a single capacitor, and the support ripple current $I_{res\max}$ = 43 × 30 = 1290A, where 43 is the ripple current that a single capacitor can support. SHE-1000-350 can be used for DC voltage measurements of up to 1000V, which meets the design of the DC voltage measurement level of the PV system.

DC TO AC Module Design

Two 1200V IGBT double-tube parallel solutions were selected to form a total power output of 500 kW, and the Infineon model FF1400R12IP4 was selected. Because this solution is a double-tube parallel solution, the dynamic current equalization of the system mainly relies on the synchronization of the particular driver to solve. The static current equalization is ensured primarily by the structural symmetry of the leading power equipment. This is achieved using Infineon's professional IGBT simulation software, IPOSIM7-3. The system is designed to account for an unevenness of 10%. Therefore, the effective output current of a single IGBT in parallel is (1176/2) × 1.1 = 647 A. A switching frequency of 3000 Hz, an output current of 1069 A, an overload current of 1176 A, a modulation ratio of 0.85, a power factor of 0.98, a bus voltage of 450 V, an output line voltage of 270 Vac, and a maximum operating ambient temperature of 55°C were used for the simulation.

Assuming the selected heat sink Rch = 0.030 K/W, when the output current was 647A, the maximum junction temperature of the IGBT was 93.9°C, the minimum junction temperature was 89.7°C, the case temperature of the IGBT was 81.5°C, the heat-sink temperature was 76.5°C, and the temperature ripple was 4.2 degrees.

The final loss is 716.6 W, of which 358.7 W is the on-off loss of the IGBT, 169.4 W is the switching loss, 71.2 W is the on-off loss of the anti-parallel diode, 66.5 W is the switching loss, and 50.72 W is the loss of the internal soldering line of the IGBT. Therefore, the total loss of the three-phase inverter was P=2 × 6×716.6=8599.2 W.

LC Parameter Design

According to references [6, 7], the formula for the inductance L_1 is:

$$L_1 = \frac{v_{dc}}{8 \times f_{sw} \times 20\% \times i_{rated}} \quad (3)$$

Substituting the parameters, v_{dc} =330V (DC-side voltage),i_{rated} = 760A (maximum pulsating current), f_{sw} =3×10^{3}Hz (switching frequency). Got. L_1 =90.4uH.

From references [7, 8], the formula for capacitance C is:

$$C = \frac{P_{rated}}{24 \times 3 \times 2 \times \pi \times f \times V_{rated}^2} \quad (4)$$

Substituting the parameters, P_{rated} = 500 KW (rated power), V_{rated} = 220V (line voltage for delta capacitor), f = 50 Hz (angular frequency). Got. $C \approx 550$uF.

Considering the above and leaving an appropriate margin for this system, the filter inductor L_1 is 100uH, and the filter capacitor C is 550uF, i.e., C2=C3=C4=550uF.

Control Strategy Design

This inverter system adopts an external and internal double closed-loop control strategy [9, 10], where the external loop system controls the DC bus voltage and the internal loop q-axis loop controls the grid-connected power factor. The internal d-axis loop achieves external loop control by controlling the active current. Modulation is carried out using the SVPWM [11, 12] algorithm, whose basic block diagram is shown in Figure 2.

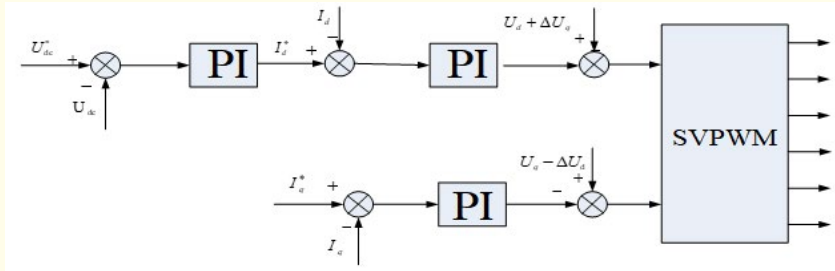

Figure 2: Basic block diagram of the control strategy.

Where U_d is the d-axis voltage, U_q is the q-axis voltage, U_{dc} is the DC bus voltage sampling value, U_{dc}^* is the given DC bus voltage value, I_d is the d-axis current sampling value, I_d^* is the given d-axis current value, and I_q^* is the q-axis current sampling value.

Maximum Power Tracking Strategy

Nonlinear Dissipative Particle Swarm Algorithm

When the illumination conditions are the same, the P-U curve of the PV panel has a single-peaked characteristic, and conventional tracking algorithms, such as the conductivity increment method [13] and the perturbation observation method [14], can achieve a better maximum power point tracking (MPPT) effect. However, the P-U characteristic curve has multi-peaked characteristics in the case of local shading by clouds, and the above conventional tracking algorithms often allow the optimal value to fall into a local optimum. To achieve multi-peaked MPPT, using intelligent optimization algorithms, such as particle swarm [15-21], to find the global power optimum is a hot research topic. In this study, the nonlinear dissipative particle swarm algorithm [22, 23] was used to overcome the shortcomings of the primary particle swarm algorithm [24, 25], which is prone to fall into a local optimum and has low search accuracy.

The mathematical expression of the nonlinear dissipative particle swarm algorithm is as follows.

$$v_i^{j+1} = \begin{cases} \omega v_i^j + c_1\xi(p_i^j - x_i^j) + c_2\eta(p_g^j - x_i^j) & \delta > k \\ rand()v_{\max} & \delta < k \end{cases} \quad (5)$$

$$x_i^{j+1} = \begin{cases} x_i^j + v_i^{j+1} & \delta < k \\ Random(l_d, u_d) & \delta > k \end{cases} \quad (6)$$

where *rand*() is a uniformly distributed random number in the interval [0, 1], v_{max} is the maximum particle velocity, ξ and η are uniformly randomly distributed between [0, 1], k is called the dissipative factor, ω is the inertia weight, and k and ω are calculated by equations (7) and (8), respectively.

$$k = (k_{max} - k_{min}) \times (iter / Gen)^n + k_{min} \quad k \in [0.01, 1] \tag{7}$$

$$\omega = -(\omega_{\max} - \omega_{\min}) \times (iter/Gen)^n + \omega_{\max} \quad \omega \in [0.95, 0.4] \tag{8}$$

where k_{max} denotes the maximum dissipative adjustment number, k_{min} denotes the minimum dissipative adjustment number, *iter* denotes the current iteration number, and *Gen* denotes the maximum iteration number. ω_{max} is the maximum inertia weight and ω_{min} is the minimum inertia weight.

This approach dynamically adjusts the trajectory of the particles while maintaining the inertia of their motion, prompting a greater chance of searching for the best position in a small area while stopping the efficiency of the particle search from decreasing as the population evolves, allowing the algorithm to operate efficiently throughout the evolutionary process.

Nonlinear Dissipative Particle Swarm Algorithm Implementing MPPT Tracking Steps

Matlab software is used to build a simulation model for the collected data, and the improved particle swarm algorithm is embedded in the simulation model to adjust and optimize the algorithm's performance.

The specific steps are as follows.

1. Use MATLAB to plot the characteristic curve of the photovoltaic cell array according to the solar cell equivalence model, as shown in Figure 3.

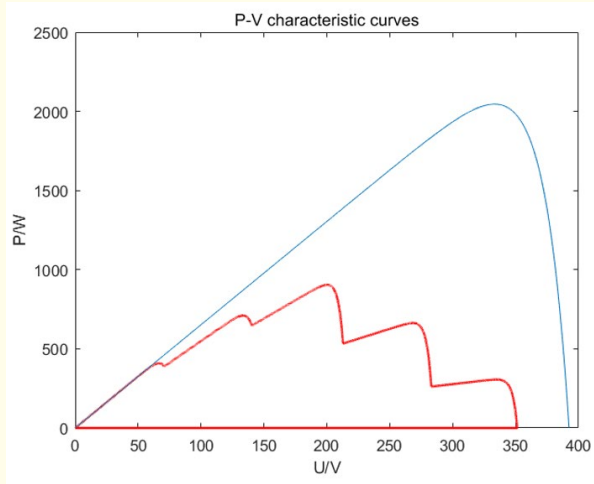

Figure 3: PV cell characteristic curve.

The blue line represents the curve for the ideal case. The red line is the PV curve of a PV cell bank connected in series. The perfect curve is not obtained because each PV cell is shaded to different degrees with multiple peaks.

2. The nonlinear diffusion particle swarm algorithm is used to find a solution to the multi-peak problem.
   Based on Eqs. (5) and (6), the main steps of the multi-peak MPPT method based on the NDPSO algorithm are as follows:
   <1> Initialize the particle population according to the initialization rules and parameter settings.
   <2> Send and execute all particles of the current generation sequentially, detect and record the output power.
   <3> Update the individual optimal particles.
   <4> Update the population optimal particles.
   <5> Calculate the perturbation of the reference voltage of the next generation according to Equation (5).
   <6> Update the particle position according to Equation (6) and go to step (2).
   The specific process is shown in Figure 4.

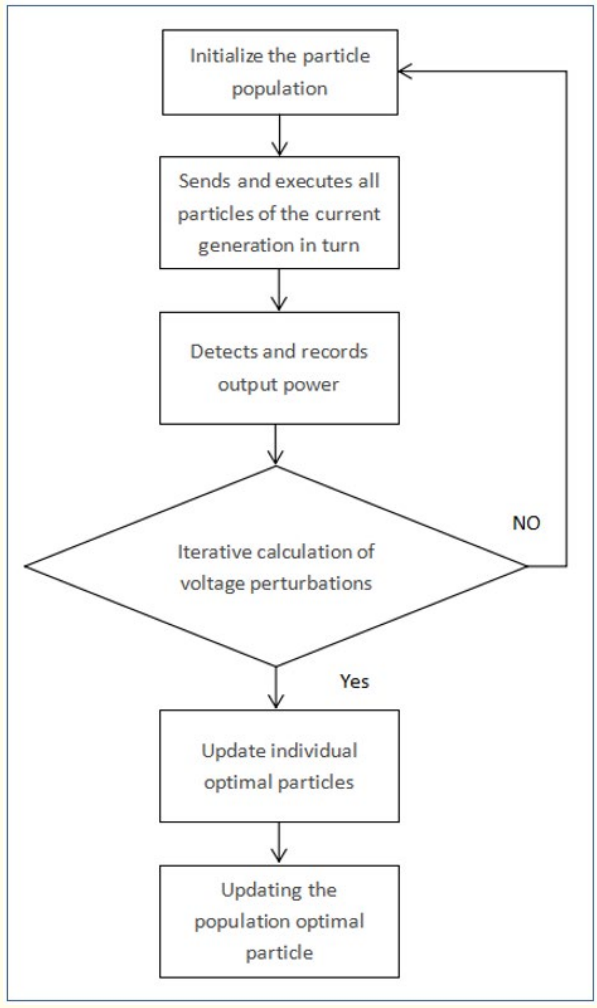

Figure 4: Flowchart of multi-peak MPPT method based on NDPSO.

If you distribute five particles evenly on the PV curve, the five particles will share the data and can lead the group to the optimal value. Apply the nonlinear dissipative particle swarm algorithm (Xu et al.,2021) to track the maximum power point. Use five particles to track this multi-peak curve at the same time. The number of iterations is 100 times. Repeat the experiment 100 times.

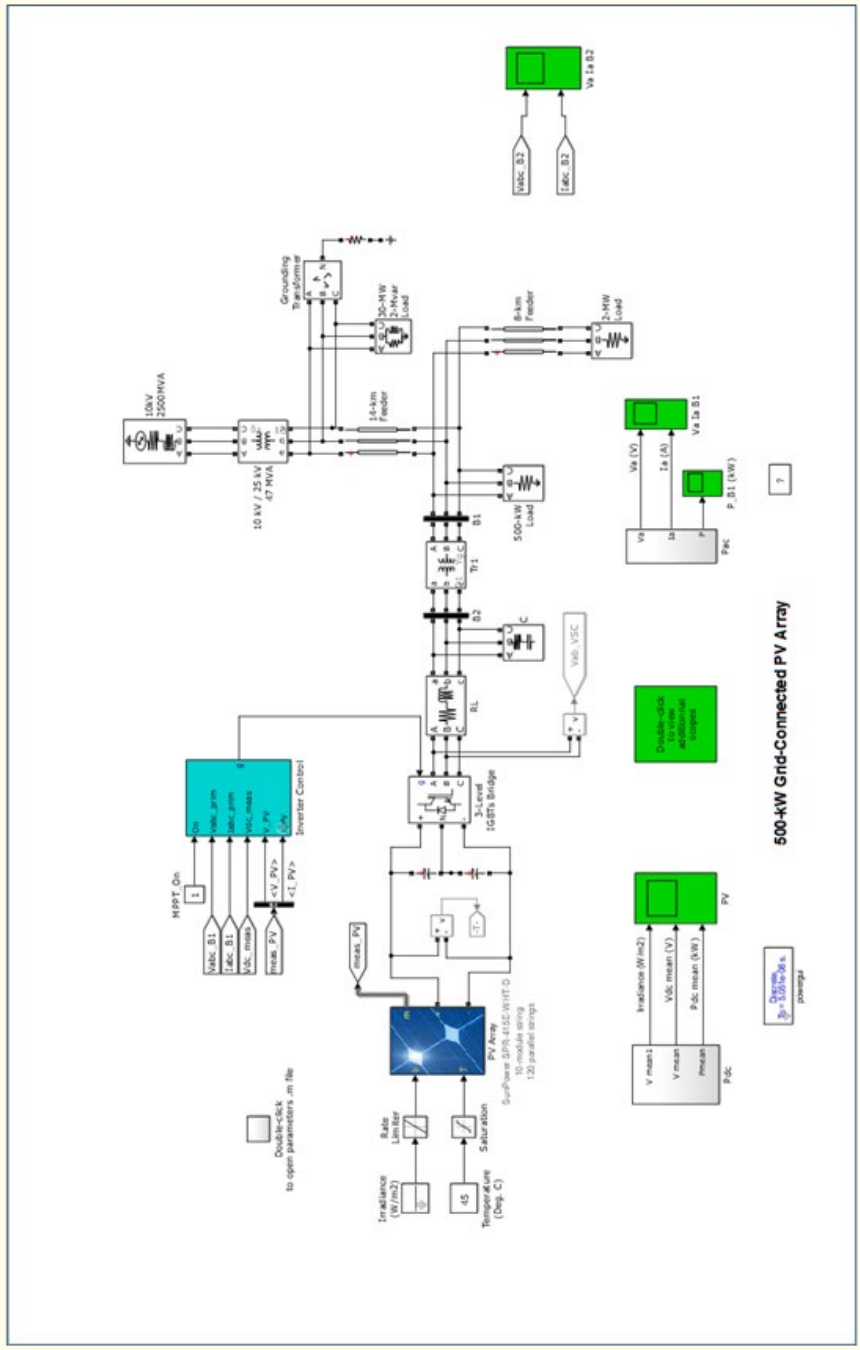

Figure 5: 500KW system simulation diagram.

Experimental Results

Photovoltaic Power Generation System Experiment

System simulation experiment

Based on the above design ideas, the Simulink simulation software simulates the 500 kW PV grid-connected inverter. A Simulink model includes a PV array, DC-DC converter, DC-AC inverter, and a scope. The configurations and connections of these modules were precisely set up to simulate the actual operating conditions of the PV power system. The simulation interface is shown in Figure 5. We select 415W photovoltaic modules in this model with the specific model SunPower SPR-415E-WHT-D. The configuration is 10 series and 120 parallel strings, resulting in a total power output of 498KW. Figures 6 and 7 show the DC side and AC-measured voltage, current, and power output waveforms. These were obtained from the PV grid-connected inverter after the Simulink simulation operation when the panels were shaded. Where: Irradiance is the variation of light intensity, Vdc represents the DC voltage, Pdc represents the DC side power, Vabc represents the AC side phase voltage, Iabc represents the AC side phase current, and power represents the AC side power.

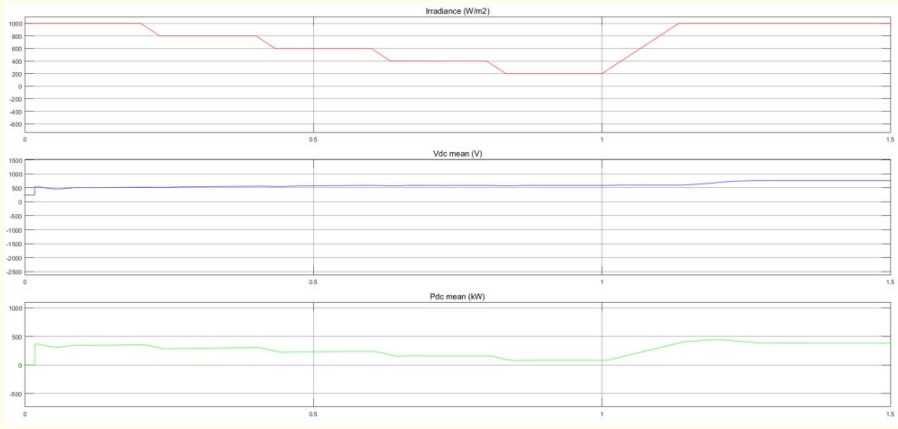

Figure 6: DC Side Waveform.

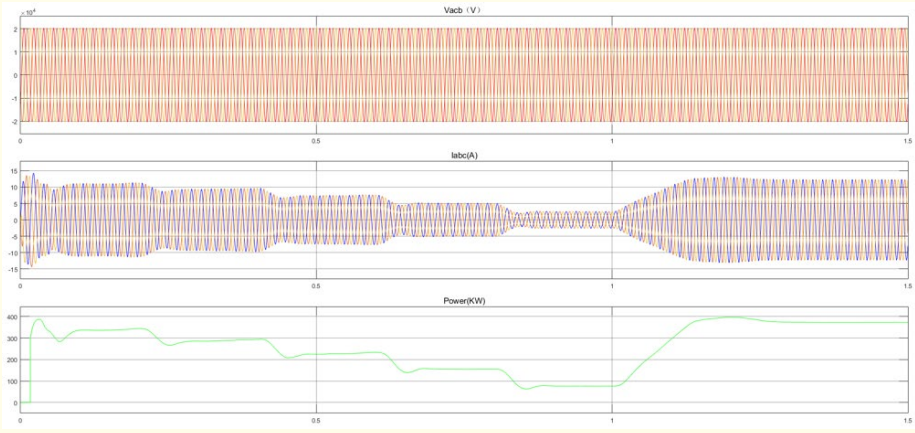

Figure 7: AC Side Waveform.

As can be seen from the simulation results in Fig. 7, the currents A, B, and C differ from each other by 120°C, which verifies the correctness of the current inner-loop control strategy. At the same time, when the shadows block the photovoltaic module, it will cause a change in the voltage and power on the DC side, which in turn will cause a change in the current and power measured on the AC side, which verifies the correctness of the system design.

Field experiment

A 500KW inverter prototype is used for field experiments. The main instruments used are an oscilloscope, power analyzer, power quality analyzer, AC current probe, and DC current probe. Figure 8 shows the inverter prototype's field operation, and Figure 9 shows its internal structure. The inverter is tested individually for conversion efficiency and harmonics.

Figure 8: Inverter field operation diagram.

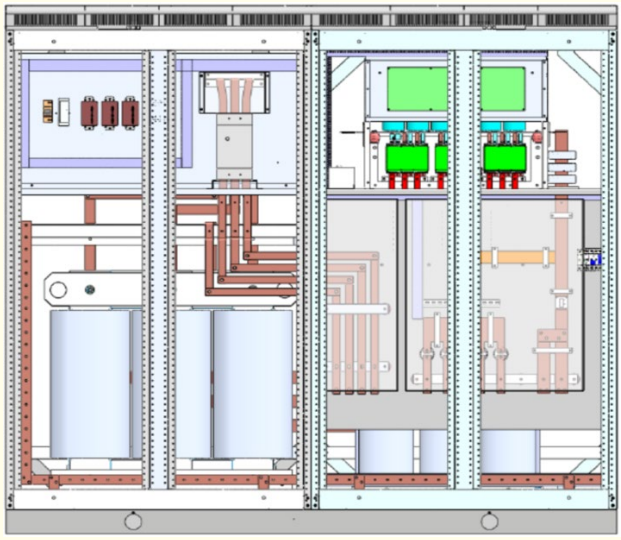

Figure 9: Inverter internal structure diagram.

Conversion Efficiency Test

The conversion efficiency is an essential parameter of the grid-connected inverter and a critical performance indicator for measuring the inverter. The test conditions in this study were as follows: the test environment was room temperature and pressure, the AC side grid information was a public three-phase grid, the DC source was a DC constant voltage source, and the load information was an active full load. The conversion efficiencies at 500V and different loads (5%, 10%, 15%, 20%, 25%, 30%, 35%, 50%, 75%, and 100%) are shown in Table 1.

Power rating (%)	*AC line voltage (V)*		*AC phase current (A)*		P_{AC} *(kW)*	*DC voltage (V)*	*DC Current (A)*	P_{DC} *(kW)*	*Efficiency (%)*
	Uab	*Ucb*	*Ia*	*Ic*					
100%	269.5	269.6	1039.4	1032.2	485.60	496.6	1006.0	499.57960	0.9720
	269.5	269.6	1039.4	1032.2	485.40	496.8	1006.2	499.88016	0.9710
75%	269.2	269.3	780.5	786.8	372.60	495.8	767.5	380.52650	0.9791
	270.2	270.2	780.2	786.3	372.70	496.3	767.6	380.95988	0.9783
50%	269.0	268.7	528.1	532.7	249.24	497.1	510.4	253.71984	0.9823
	269.3	269.2	527.8	532.6	249.12	497.7	509.5	253.57815	0.9824
30%	269.9	269.6	317.8	318.8	150.72	498.2	306.5	152.69830	0.9870
	270.0	269.8	317.7	321.4	150.75	498.1	306.6	152.71746	0.9871
25%	269.9	269.6	265.4	269.2	125.57	496.7	256.5	127.40355	0.9856
	270.0	269.7	265.4	269.0	125.53	497.4	256.1	127.38414	0.9854
20%	269.7	269.5	213.2	216.4	100.27	497.8	204.7	101.89966	0.9840
	269.0	269.4	213.1	216.5	100.29	497.7	204.6	101.82942	0.9848
15%	270.5	270.3	161.5	164.7	75.17	497.2	154.2	76.66824	0.9804
	270.5	270.2	161.6	164.6	75.30	498.6	154.1	76.83426	0.9800
10%	270.6	270.2	111.6	114.3	50.29	498.5	103.6	51.64460	0.9737
	270.5	270.1	111.9	114.5	50.28	497.8	103.7	51.62186	0.9740
5%	270.3	270.0	67.0	68.7	25.22	498.4	52.5	26.16600	0.9638
	270.5	270.3	67.2	68.7	25.21	498.1	52.6	26.20006	0.9622

Table 1: Inverter conversion efficiency under different load conditions.

where P_{AC} is the output power of the inverter at the AC port; P_{DC} is the input power of the inverter at the DC port; Uab and Ucb are the AC line voltages; and Ia and Ic are the AC phase currents. The maximum conversion efficiency point can be obtained at 30% of the load power, and its maximum conversion efficiency is 98.71%. According to the European efficiency formula(9), the data in Table 2 give a European efficiency weighted value of 98.09%.

$$\eta = \eta_{5\%} \times 0.03 + \eta_{10\%} \times 0.06 + \eta_{20\%} \times 0.13 + \eta_{30\%} \times 0.10 + \eta_{50\%} \times 0.48 + \eta_{100\%} \times 0.20 \quad (9)$$

Inverter European efficiency calculation table						
Rated PowerPoint	5.00%	10.00%	20.00%	30.00%	50.00%	100.00%
Weighting factor	0.03	0.06	0.13	0.10	0.48	0.20
Test point efficiency values	96.38%	97.4%	98.48%	98.71%	98.24	97.2%
Efficiency Europe	98.09%					

Table 2: Inverter European efficiency calculation table.

Harmonic Testing

The inverter should ensure that it does not cause excessive distortion of the grid voltage waveform. It must also prevent excessive harmonic currents from being injected into the grid during operation. This ensures no adverse effects occur for other equipment connected to the grid. Following the relevant regulations for inverter certification, the total harmonic distortion rate of the current injected into the grid is limited to 5% when the inverter operates at rated power. The limit values for the content of odd harmonic currents are listed in Table 3, and the limit values for the content of even harmonic currents are listed in Table 4. The harmonic current injected into the grid under any load conditions should not exceed the harmonic current value injected when the inverter operates at rated power.

Number of odd harmonics	*Limits of content rate (%)*
3rd-9th	4.0
11th-15th	2.0
17th-21st	1.5
23rd-33rd	0.6
35th and above	0.3

Table 3: Limit values for odd harmonic current content.

Number of even harmonics	*Limits of content rate (%)*
2nd-10th	1.0
12th-16th	0.5
18th-22nd	0.375
24th-34th	0.15
36th and above	0.075

Table 4: Limits on the content of even harmonic currents.

The test environment was maintained at room temperature and pressure. The AC-side grid information is a public three-phase grid. The DC source was a constant voltage DC source. The load information was the active full load. The leading test equipment was a power quality analyzer (FLUKE-435). The harmonic value and the rate of content of the currents were measured at a given value of 100% AC current (repeated three times; each test time was 150s, and the average value was taken), as shown in Tables 5 and 6.

From Table 5 and Table 6, we can obtain the maximum current harmonic value and content rate for each phase: for THDIa = 6.81A, its maximum content rate is 0.64%. THDIb = 6.02A, its maximum content rate is 0.56%, and THDIc = 6.31A, its maximum content rate is 0.59%. The maximum THD in the three-phase currents was less than 1%, and the contents of all harmonics were below the requirements of the certification regulations.

AC phase current			Ia		Ib		Ic	
	Limiting value of content rate	Secondary	Harmonic values	Content rate	Harmonic values	Content rate	Harmonic values	Content rate
Odd times	4.00%	4.00%	1.07	0.10%	5.45	0.51%	4.46	0.42%
		4.00%	6.81	0.64%	6.02	0.56%	6.31	0.59%
		4.00%	0.05	0.00%	0.09	0.01%	0.32	0.03%
	2.00%	2.00%	2.05	0.19%	2.59	0.24%	0.55	0.05%
		2.00%	1.61	0.15%	3.02	0.28%	0.87	0.08%
		2.00%	0.52	0.05%	0.89	0.08%	0.13	0.01%
	1.50%	1.50%	1.46	0.14%	0.67	0.06%	1.03	0.10%
		1.50%	0.93	0.09%	0.17	0.02%	0.68	0.06%
		1.50%	0.59	0.06%	0.19	0.02%	0	0.00%
	0.60%	0.60%	0.51	0.05%	0.55	0.05%	1.28	0.12%
		0.60%	0.64	0.06%	0.24	0.02%	0.26	0.02%
		0.60%	0.13	0.01%	0.37	0.03%	0.08	0.01%
	0.30%	0.30%	0.22	0.02%	0.28	0.03%	0.28	0.03%
		0.30%	0.23	0.02%	0.22	0.03%	0.23	0.03%
		0.30%	0.2	0.02%	0.24	0.03%	0.23	0.03%

Table 5: Odd harmonic values and inclusion rates at 100% of the given current value.

AC phase current			Ia		Ib		Ic	
	Limiting value of content rate	Secondary	Harmonic values	Content rate	Harmonic values	Content rate	Harmonic values	Content rate
Even times	1.00%	1.00%	0.79	0.07%	1.3	0.12%	0.9	0.08%
		1.00%	1.44	0.13%	3.1	0.29%	2.76	0.26%
		1.00%	0.28	0.03%	0.95	0.09%	1.09	0.10%
	0.50%	0.50%	0.08	0.01%	0.21	0.02%	0.13	0.01%
		0.50%	0.67	0.06%	0.15	0.01%	0.35	0.03%
		0.50%	1.28	0.12%	0.33	0.03%	0.26	0.02%
	0.37%	0.37%	0.32	0.03%	0.2	0.02%	0.14	0.01%
		0.37%	0.27	0.03%	0.37	0.03%	0.25	0.02%
		0.37%	0.28	0.03%	0.61	0.06%	0.18	0.02%
	0.15%	0.15%	0.28	0.03%	0.95	0.09%	1.09	0.10%
		0.15%	0.72	0.07%	0.76	0.07%	0.58	0.05%
		0.15%	0.16	0.01%	0.08	0.01%	0.08	0.01%
	0.08%	0.08%	0.16	0.01%	0.1	0.01%	0.09	0.01%
		0.08%	0.19	0.01%	0.1	0.01%	0.1	0.01%
		0.08%	0.15	0.01%	0.1	0.01%	0.09	0.01%

Table 6: Even harmonic values and inclusion rates at 100% of the given current value.

Experimental multi-peak MPPT control strategy based on improved particle swarm algorithm
Simulation modeling of mismatch

There are many reasons for the local shading of PV modules, such as the surrounding buildings, trees, clouds, dust, fallen leaves, and other factors. According to the shading effect on PV modules, it can be divided into the following two cases:

1. One or more isolated shadow points, the cause of which may be falling leaves, stains, and a relatively large range of variation in equivalent irradiance attenuation. The shaded spots may be distributed within one or more parallel diode branches, as shown in Figure 10, where the black dots represent the solar cells at the shaded spots, and the non-black dots represent the solar cells that receive light typically.
2. A continuous patch of shadows caused by surrounding buildings, trees, clouds, etc. The shadows start from the edges of the module and cover a continuous patch of it. The specific form is shown in Fig. 11.

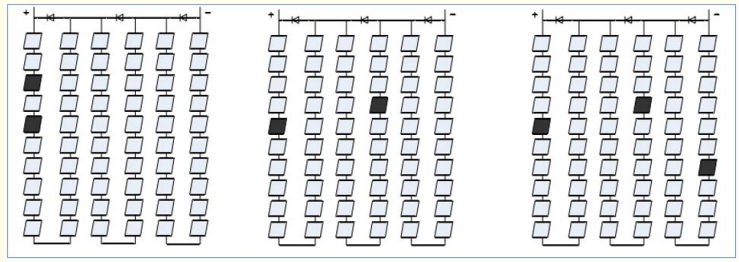

Figure 10: Distribution of isolated shaded points.

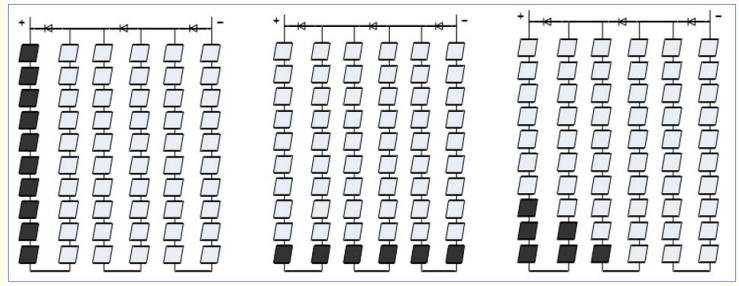

Figure 11: Distribution of continuous shadows.

It is shown that the MPP of the PV module under uniform irradiance is located at 0.7-0.82 times the open-circuit voltage (Voc) and 0.85±0.07 times the short-circuit current (Isc). The photovoltaic current is proportional to the irradiance, the short-circuit current is approximately equal to the photovoltaic current, and the MPP current is proportional to the short-circuit current, so it can be considered that the MPP current is approximately proportional to the irradiance. The irradiance settings for each solar cell group (five groups in total) are used to analyze the peak point distribution pattern of PV modules under local shadows. The irradiance of each cell group of the PV module is shown in Table 7, and there are three types of scenarios: Scenario 1 is that the ratio of the two similar irradiances is close to 0.85; Scenario 2 is that the ratio of the two similar irradiances is much less than 0.85, and Scenario 3 is that the ratio of the two similar irradiances is close to 0.85 and much less than 0.85. The temperature parameter is uniformly set to 25°C, and the corresponding output P-V and I-V curves and peak point distribution are shown in Figs. 12-14.

t=25℃	*Battery group1*	*Battery group2*	*Battery group3*	*Battery group4*	*Battery group5*
Scenario 1	1000	800	600	400	200
Scenario 2	1000	600	300	150	75
Scenario 3	1000	850	720	400	150

Table 7: Irradiance of each group of PV cells of PV module under local shadows (W/m2).

As can be seen from Figs. 12-14, the peak point distribution of the PV module has the following characteristics:

1. Taking the PV cell strings connected in parallel with the bypass diode as a group, the possible peak points are located at about n*0.8Voc, where Voc is the open-circuit voltage of the PV cell strings, and the value of n ranges from a natural number less than or equal to the total number of groups;
2. Two peak point power values are very close to the case; GMPP may be the two points in one of the GMPP may be one of the two points, or it may be other than the two points;
3. The current decreases as the voltage increases for the same I-V curve.

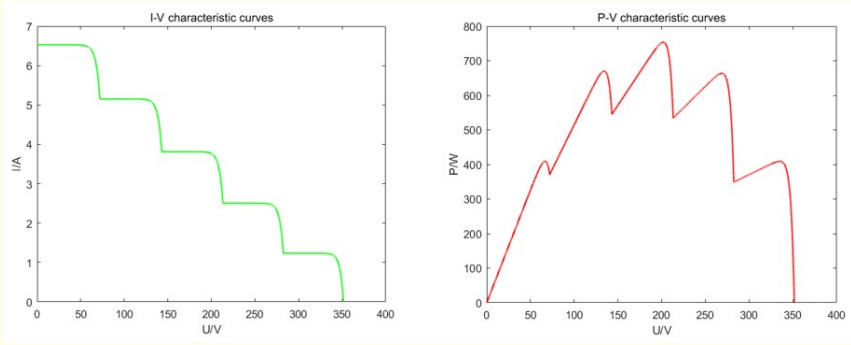

Figure 12: I-V and P-V characteristic curves (Scenario 1).

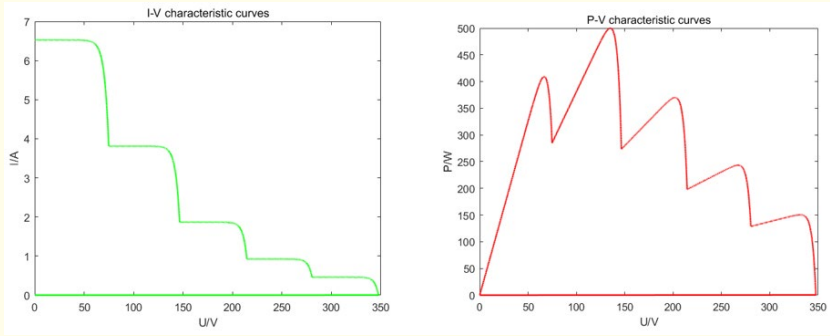

Figure 13: I-V and P-V characteristic curves (Scenario 2).

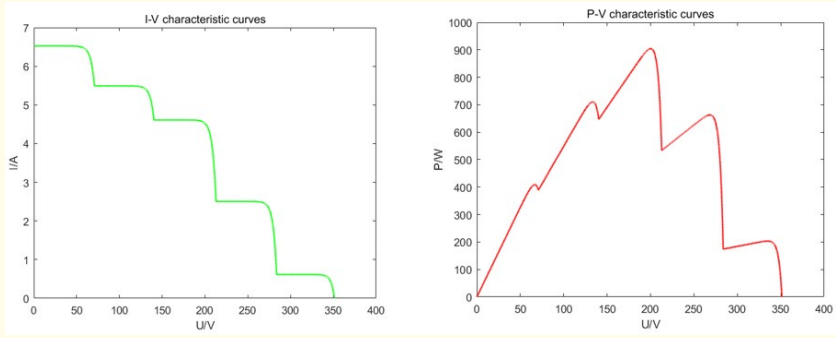

Figure 14: I-V and P-V characteristic curves (Scenario 3).

When two PV modules are connected in parallel, the irradiance settings of the module and the module are different, and the irradiance of the single module is one of the cases in Table 7; the corresponding output I-V and P-V curves and peak point distribution are shown in Figs. 15-17. From Figs. 15-17, it can be seen that the possible peak point is still located at about n*0.8 Voc, and there may be several peak points with very close power values. Therefore, the parallel connection of the same type of components does not significantly change the peak distribution pattern.

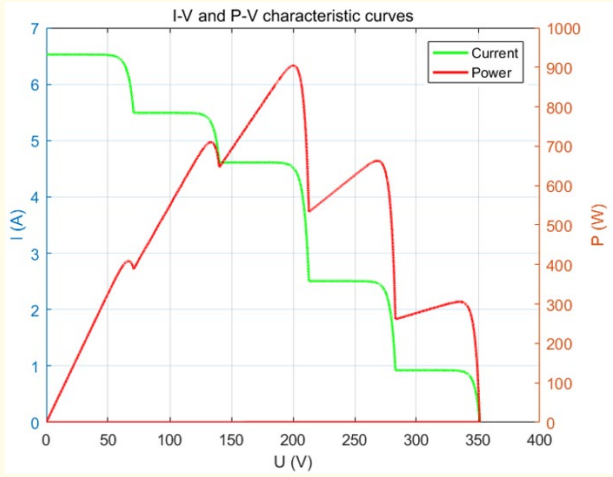

Figure 15: The irradiance is a combination of cases 1 and 2.

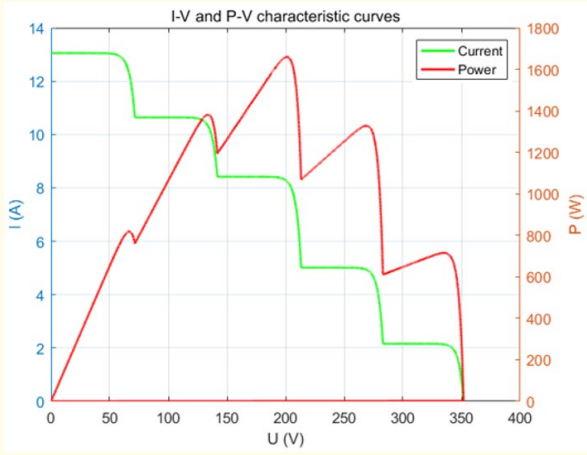

Figure 16: The irradiance is a combination of cases 1 and 3.

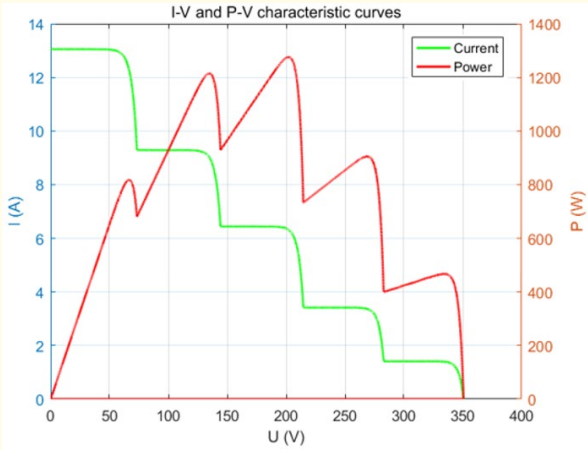

Figure 17: The irradiance is a combination of cases 2 and 3.

From the above analysis, it can be seen that in the multi-peak scenario, two peak points may exist with very close power values, and more complexly, the GMPP may be one of these two peak points or some other peak point. Therefore, it isn't easy to locate the GMPP region quickly and accurately by simple methods, and the fast scanning strategy of the P-V curve becomes the core of the multi-peak MPPT method.

Maximum power point tracking simulation experiment comparison

Most of the time, the PV system still works in the single-peak case. The I-V and P-V curves in the single-peak case are shown in Fig. 18. The multi-peak case only occurs when the module parameters are mismatched, or there are local shadows. The I-V and P-V curves are shown in Fig. 19.

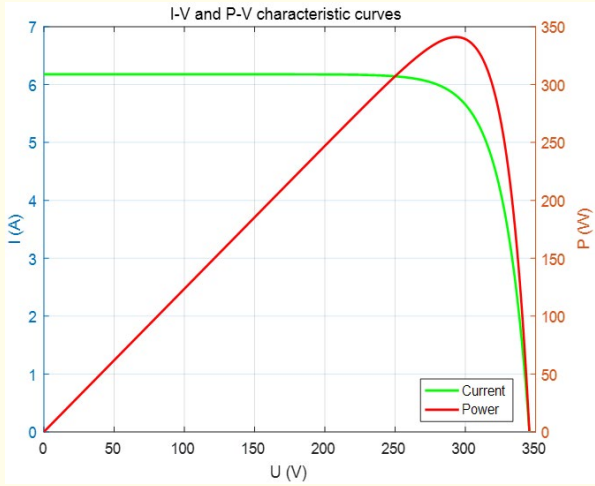

Figure 18: I-V and P-V curves for single-peak case.

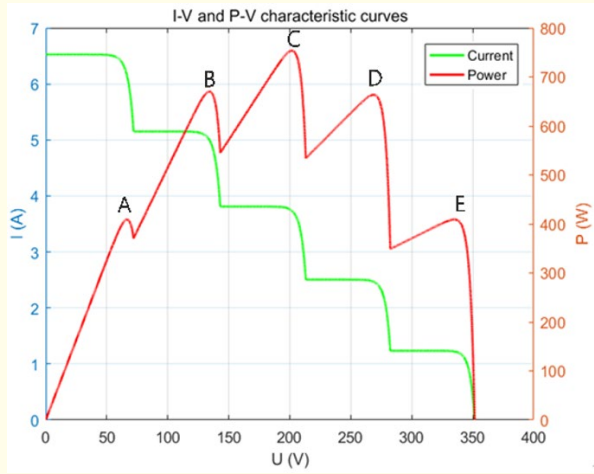

Figure 19: I-V and P-V curves in the multi-peak case.

For the single-peak condition, the I-V and P-V curves are optimized using the nonlinear dissipative particle swarm algorithm, and the optimization results are shown in Figs. 20-21, of which Fig. 20 is the optimization particle dynamics process diagram. Figure 21 shows the final result of optimization.

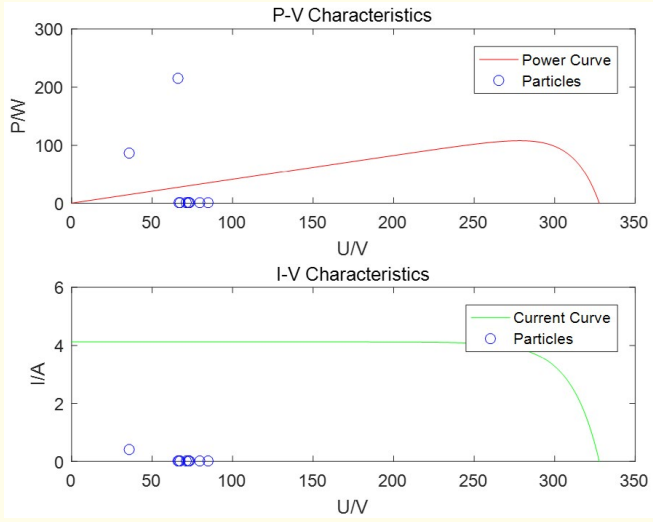

Figure 20: Optimization particle dynamics.

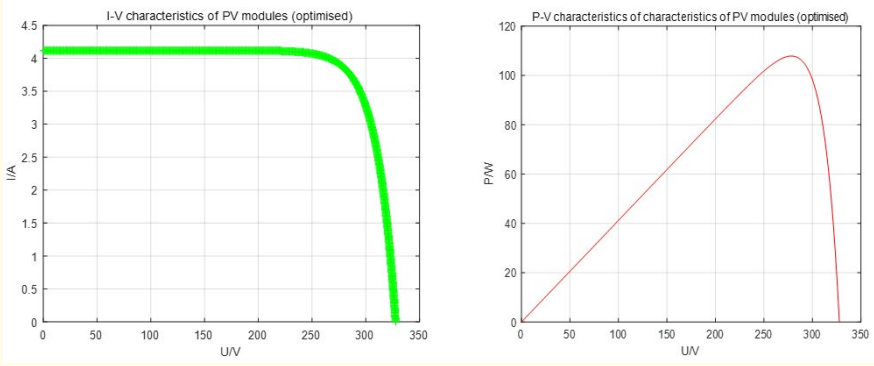

Figure 21: Optimization result

Under the single-peak situation, applying the nonlinear dissipative particle swarm algorithm and the elementary particle swarm algorithm to track the maximum power point, repeat the experiment 100 times, and the experimental results show that these two algorithms can achieve the tracking effect very well and the difference in their tracking effect is not apparent.

Figure 19 shows the multi-peak IV and P-V curves. The P-V curve has five peaks: A, B, C, D, and E, and only C is the global peak point. In the following, the I-V and P-V curves in Fig. 19 and the different irradiance settings in Table 7 will be used as the basis to evaluate the MPPT tracking performance of the two methods, NDPSO and PSO, in the multi-peak case.

The nonlinear dissipative particle swarm algorithm and elementary particle swarm algorithm are also applied to track the maximum power point, and five particles are used to track the multi-peak curve simultaneously, with 100 iterations and 100 repetitions of the experiment. The results are shown in Table 8, and the tracking effect of NDPSO is shown in Figs. 22-24.

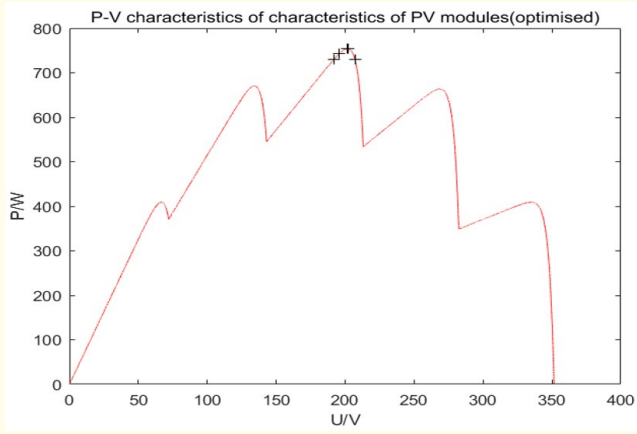

Figure 22: Tracking effect of NDPSO in irradiance as case 1.

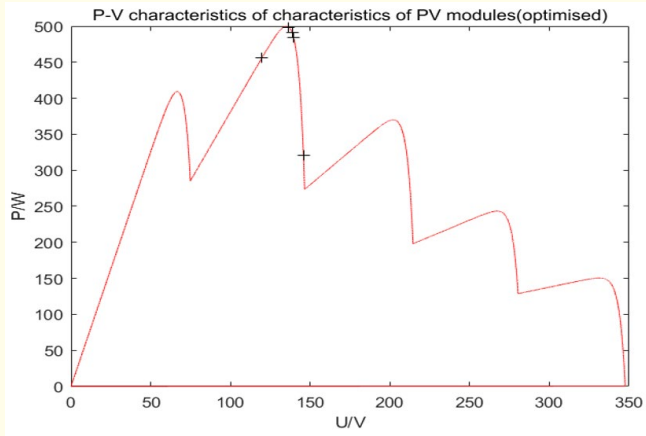

Figure 23: Tracking effect of NDPSO in irradiance as case 2.

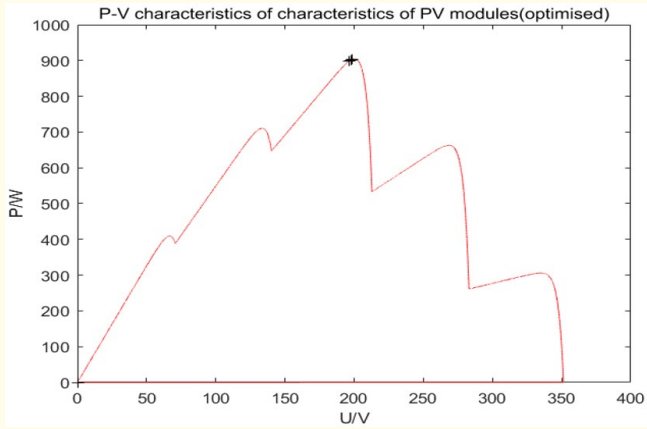

Figure 24: Tracking effect of NDPSO in irradiance as case 3.

From Table 8, it can be seen that the NDPSO algorithm can quickly track PV's maximum power point. Its algorithm implementation time and particle tracking efficiency are significantly better than those of the primary particle swarm algorithm. The effect is pronounced, and it is worth promoting.

Irradiance	***Algorithm***	***Achieve optimal particle count at the same time***	***5 particles***	***4 particles***	***3 particles***	***2 particles***	***1 particle***
Scenario 1	NDPSO	Number of times (times)	70	82	91	98	100
		Number of iterations to reach the optimal value the fastest (times)					9
	PSO	Number of times (times)	48	65	82	88	92
		Number of iterations to reach the optimal value the fastest (times)					28
Scenario 2	NDPSO	Number of times (times)	65	78	90	94	100
		Number of iterations to reach the optimal value the fastest (times)					8
	PSO	Number of times (times)	52	70	80	90	95
		Number of iterations to reach the optimal value the fastest (times)					48
Scenario 3	NDPSO	Number of times (times)	72	79	93	96	100
		Number of iterations to reach the optimal value the fastest (times)					12
	PSO	Number of times (times)	50	62	78	90	94
		Number of iterations to reach the optimal value the fastest (times)					36

Table 8: Particle tracking results.

Comparison of actual measurement of power generation effect

The main factors affecting the change in the maximum power point of the panels are the changes in light and temperature. The data in Fig. 25- 27 are obtained from the measured data of a 1MW PV power plant in Pingyang. Fig. 25 shows the MPPT tracking effect when the light changes rapidly, Fig. 26 shows the MPPT tracking effect when the temperature difference varies greatly, and Fig. 27 shows the MPPT tracking effect when the temperature difference and the light changes are slow. The plant consists of two 500KW inverters (from Zhejiang Efisen), one of which adopts the MPPT algorithm (P-ndpso) designed in this system cum NDPSO algorithm for designing the maximum power point tracking, and the other adopts the enterprise's design scheme (P-owm) cum perturbation observation method for designing the maximum power point tracking. The results show that the inverter designed with this system responds faster to the changes in solar insolation under different weather and has a higher PV power generation efficiency under local shadow shading than the system designed with the perturbation observation method.

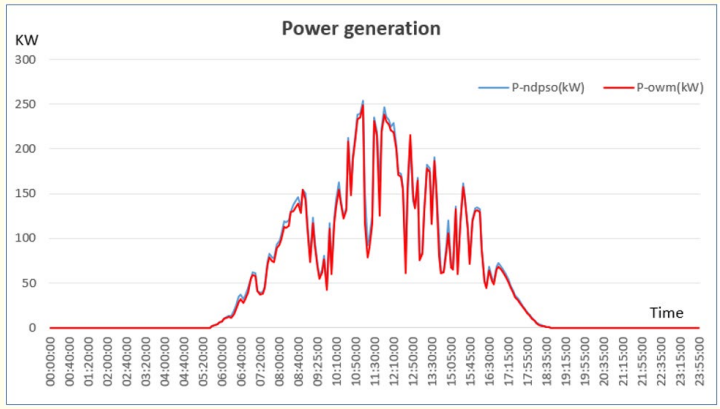

Figure 25: MPPT tracking on August 12, 2022.

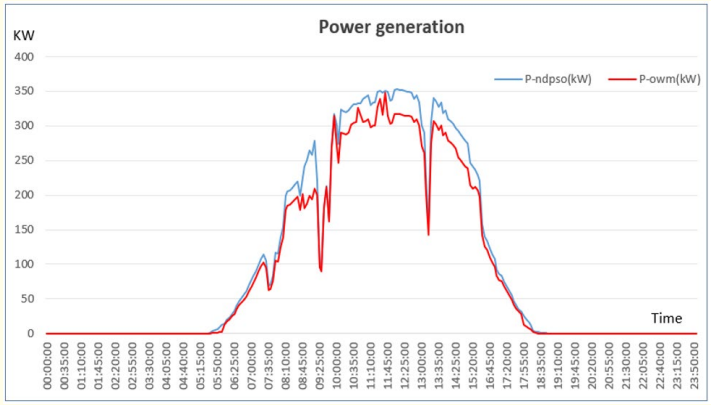

Figure 26: MPPT tracking on August 13, 2022.

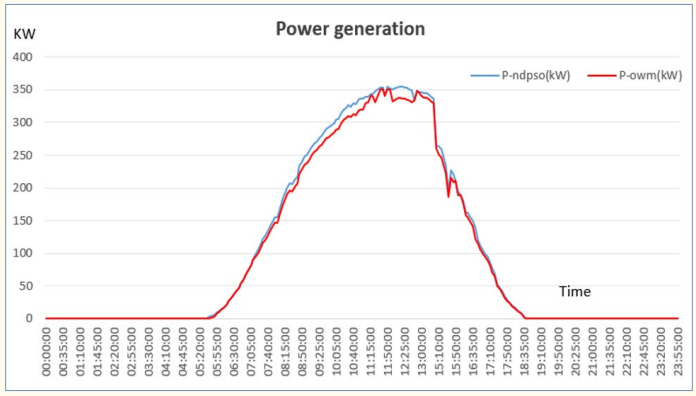

Figure 27: MPPT tracking on August 14, 2022.

Conclusion

Based on the analysis of the working principle of the high-power PV grid-connected inverter, this paper takes a 500 kW PV grid-connected inverter as an example and focuses on the design of critical parts such as the DC support capacitor, DC-to-AC module, and LC filter module. The control strategy and MPPT tracking strategy of this system are briefly introduced. The experimental results show that the inverter has a high conversion efficiency, good harmonic suppression, and good MPPT tracking effect, which have high application and promotion value.

References

1. Ding K., et al. "A novel single-phase asymmetric 5-level inverter". Proceedings of The CSEE 11 (2004): 116-120.
2. Guo LL., et al. "Nonparametric sliding mode predictive control strategy for a three-phase LCL grid-connected inverter". Power System Protection and Control 50 (2022): 72-82.
3. Qiu JL., et al. "Leakage current suppression and balance control of neutral point potential for three-level transformerless inverter". Automation of Electric Power Systems 45 (2021): 161-170.
4. Liang CS. "Research on the Selection of Centralized Inverter and String Inverter in Large-scale Photovoltaic Power Station". Telecom Power Technology 37 (2020): 283-285.
5. Zhang X., et al. "Overview of high efficiency photovoltaic inverter". Power Technology 40 (2016): 931-934.
6. Prasad VH. "Analysis and comparison of space vector modulation schemes for three-leg and four-leg voltage source inverters". Master dissertation, Virginia Polytechnic Institute and State University, Blacksburg, VA (1997).
7. Qiu XN, Xu QH and Zhang XJ. "Design of 100kW photovoltaic grid connected inverter system". Control Engineering 20 (2013): 72-75.
8. Wang TCY., et al. "Output filter design for a grid-interconnected three-phase inverter". Power Electronics Specialist Conference (2003): 779-784.
9. Xu DH. "Modeling and control of power electronics system". Beijing, China Machine Press (2005).
10. Chen K, Yang Y and Shang JP. "Research on control strategy of grid-connected inverter in photovoltaic power system". Process Automation Instrumentation 41 (2020): 46-50.
11. Zhao H and Hu RJ. "Space-Vector Pulse Width Modulation and it's Simulation Based on Simulink". Transactions of China Electrotechnical Society 30 (2015): 350-353.

12. Gao Z., et al. "A carrier based SVPWM Begins with Zero Voltage for Three-Level Neutral Point Clamped Converter". Transactions of China Electrotechnical Society 35 (2020): 2194-2205.
13. Tang JZ, Wang CL and Fang XF. "MPPT implementation strategy based on the conductance increment method". Power Electronics 45 (2011): 73-75.
14. Ni Y and Hao SX. "Motion characteristics analysis of P&Q control MPPT system". Acta Electronica Sinica 43 (2015): 1388-1394.
15. Kou GY and Wei GH. "Hybrid Particle Swarm Optimization-based Modeling of Wireless Sensor Network Coverage Optimization". International Journal of Advanced Computer Science and Applications 14 (2023): 982-991.
16. Lu HX., et al. "A particle swarm optimization algorithm based on deep deterministic policy gradient". Journal of University of Electronic Science and Technology of China 50 (2021): 199-206.
17. Rauf HT., et al. "Particle Swarm Optimization with Probability Sequence for Global Optimization". IEEE Access 8 (2020): 110535-110549.
18. Guo L and Abdul NMM. "Design and Evaluation of Fuzzy Adaptive Particle Swarm Optimization Based Maximum Power Point Tracking on Photovoltaic System Under Partial Shading Conditions". Frontiers in Energy Research 9 (2021): 712175.
19. Li Z., et al. "Study of photovoltaic multi-mode maximum power point tracking based on improved quantum particle swarm algorithm". Acta Energiae Solaris Sinica 42 (2021): 221-229.
20. Zhang Y., et al. "Photovoltaic MPPT algorithm based on adaptive particle swarm optimization neural-fuzzy control". Journal of Intelligent and Fuzzy Systems 44 (2023): 341-351.
21. Zhao B., et al. "Multi-peak MPPT control of PV array based on improved ALO algorithm". Acta Energiae Solaris Sinica 42 (2021): 132-139.
22. Zheng LW, Liu SR and Xu QH. "Constant power flow control at the grid-connected point of photovoltaic microgrid based on nonlinear diffusion particle swarm optimization". Power System Technology 34 (2010): 152-156.
23. Xu QH, Wu TH and Wang WW. "Nonlinear dissipative particle swarm algorithm and its applications". IEEE ACCESS 9 (2021): 158862-158871.
24. Kennedy J and Eberhart RC. "Particle swarm optimization". Proceedings of the IEEE International Conference on Neural Networks (1995): 1942-1948.
25. Shi Y and Eberhart R. "Empirical study of particle swarm optimization". International Conference on Evolutionary Computation (1999): 1945-1950.